NIST Technical Note
NIST TN 2383

Hall Resistance, van der Pauw Test Method – Tutorial

Jan Obrzut

This publication is available free of charge from:
https://doi.org/10.6028/NIST.TN.2383

NATIONAL INSTITUTE OF STANDARDS AND TECHNOLOGY
U.S. DEPARTMENT OF COMMERCE

NIST Technical Note
NIST TN 2383

Hall Resistance, van der Pauw Test Method – Tutorial

Jan Obrzut
Materials Science and Engineering Division
Material Measurement Laboratory

This publication is available free of charge from:
https://doi.org/10.6028/NIST.TN.2383

September 2026

U.S. Department of Commerce
Howard Lutnick, Secretary

National Institute of Standards and Technology
Arvind Raman, NIST Director and Under Secretary of Commerce for Standards and Technology

NIST TN 2383
September 2026

Certain equipment, instruments, software, or materials, commercial or non-commercial, are identified in this paper in order to specify the experimental procedure adequately. Such identification does not imply recommendation or endorsement of any product or service by NIST, nor does it imply that the materials or equipment identified are necessarily the best available for the purpose.

Publication History
Approved by the NIST Editorial Review Board on 2026-09-16

How to Cite this NIST Technical Series Publication
Obrzut J (2026) Hall Resistance, van der Pauw Test Method - Tutorial. (National Institute of Standards and Technology, Gaithersburg, MD), NIST Technical Note (TN) NIST TN 2383. https://doi.org/10.6028/NIST.TN.2383

Author ORCID iDs
Jan Obrzut: 0000-0001-6667-9712

Contact Information
jan.obrzut@nist.gov

Abstract

The van der Pauw Hall Resistance test method offers exceptional insight into intrinsic electronic properties of nanomaterials, including graphene, and those of few layers graphene. In comparison, the measurements in accordance with the classical Hall-bar resistance standards require complex sample preparation procedures, test structure, and skills that often are not available to manufacturers of the Graphene related materials and products, such as graphene flakes reprocessed into ink formulations and 2D composites. The van der Pauw method employs a simple symmetric testing structure for which the geometrical dimensions do not need to be known. The presented procedure is based on simplified sets of the classical Hall Resistance mathematical equations permitting Hall voltage data fitting to linear plots as a function of magnetic field. Such graphical representation of data simplifies evaluation of statistical uncertainty, allows identification of the majority charge carriers and distinguishing between semiconducting and metallic character of graphene related materials. In the case of truly 2D charge transport, a quantized resistance can be identified. The method is suitable for quality control of practically relevant nano-carbon materials such as graphene inks and composites that are obtained from a wide range of scalable, low-cost, and commercial technologies. Despite its simplicity the method can be used to identify quantum Hall resistance in the case where the charge transport is truly confined to two dimensions (2D) and becomes quantized.

Keywords

Charge carriers density; carriers; majority; carriers mobility; Graphene; Hall resistance; 2D Materials; Nono-electronics.

Table of Contents

1. Introduction

Graphene is commonly produced by mechanical exfoliation, chemical vapor deposition (CVD), and Epitaxial growth on silicon carbide. Its extended π-conjugated network enables high charge-carrier mobility and gives rise to exceptional electronic properties [1–3]. While single-layer graphene (SLG) is of fundamental scientific importance, few-layer graphene (FLG) has emerged as a practically relevant material for a broad range of scalable, low-cost, and commercially viable technologies [3–7].

Reliable characterization of the electrical transport properties of graphene and FLG is important for both research and manufacturing. The van der Pauw Hall resistance method [9,10,15,16] provides direct information about intrinsic electronic properties, including the sign, concentration, and mobility of the majority charge carriers. In graphene-related materials, identification of the majority carrier type can also help distinguish metallic graphene from semiconducting graphite or graphitic by-products that may remain after processing.

In comparison, measurements based on conventional Hall-bar structures generally require more complex sample preparation, precisely defined device geometries, dedicated test structures, and specialized fabrication skills. These requirements may not be readily available to manufacturers of graphene-related materials and products, particularly when graphene flakes are processed into inks, coatings, or two-dimensional composites.

The van der Pauw method provides a simpler alternative by employing a symmetric test structure [9,10,15] for which the geometrical dimensions of the specimen do not need to be known. The procedure presented here is based on simplified forms of the classical Hall resistance equations and permits Hall-voltage data to be represented as linear functions of applied magnetic field. This graphical representation facilitates evaluation of statistical uncertainty and determination of the polarity, concentration, and mobility of the majority charge carriers. These parameters provide a practical means of assessing the electronic character and material quality of graphene-based products, including the presence of semiconducting graphitic phases or other processing by-products.

Despite its relative simplicity, the method is also applicable when charge transport is effectively confined to two dimensions. Under appropriate conditions, quantized Hall resistance associated with the quantum Hall effect can be identified. The van der Pauw Hall resistance method is therefore suitable for both fundamental characterization and quality control of technologically relevant nano-carbon materials, including graphene inks and composites [1,2,11], produced using scalable and cost-effective manufacturing technologies.

2. Theoretical background

2.1. Hall effect

The principle of the Hall effect [8,9] states that when a driving current (I_x) is applied to a current-carrying conductor or a semiconductor and introduced to a perpendicular magnetic field, B_z, a lateral voltage V_{xy} due to Lorenz force can be measured at the right angle to the current path I_x. This effect of sensing a measurable of V_{xy} – the Hall Voltage - is known as the Hall effect. Figure 1 illustrates a diagram of the testing structure and the corresponding measurable Hall parameters B_z, V_{xy} and I_x.

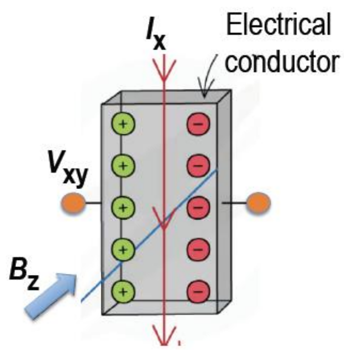

Figure 1. Illustration of the Hall effect: Under magnetic field (B_z) the positive and negative charges of current (I_x) drift to opposite sides of the conductor producing a Hall voltage (V_{xy}).

2.2. The following definitions are used in this tutorial

Hall Coefficient (R_H)
the Hall coefficient is a material specific property defining the strength of the Hall effect, representing the ratio of the Hall voltage (V_{xy}) over the driving current (I_x) and the magnetic field (B_z)

Hall Voltage (V_{xy})
the transverse voltage V_{xy} developed across a constant driving current, I_x, under perpendicular magnetic field B_z. (Figure 1).

Driving current (I_x)
driving current passed longitudinally through the testing structure illustrated in Figure1)

Voltage (V_{xx})
V_{xx} is the voltage drop measured between terminals parallel of the current I_x,

Hall resistance (R_{xy})
R_{xy} is the ratio of the Hall voltage, V_{xy}, over the driving current, I_x under perpendicular magnetic field, B_z.

Sheet resistance (R_{xx})

R_{xx} is the ratio of the voltage V_{xx} measured at the driving current terminals divided by I_x without magnetic field
$R_{xx} = V_{xx} / I_x$, $B_z = 0$.

resistance (R_{xx}) is the surface (sheet) resistance

For nano-scale materials equations (1) – (4) define in two dimensions (2D) the classical relations between the Hall coefficient (R_H) and the corresponding expressions for Hall resistance (R_{xy}) elementary charge (q), charge carriers mobility (μ) and their density (n_s) [8, 9]

$$R_H = V_{xy} / (I_x B_z) = 1/(n_s q) \quad (1)$$

$$R_{xy} = V_{xy} / I_x \quad (2)$$

$$\mu = (R_H / R_{xx}) \quad (3)$$

$$n_s = I_x B_z / (q V_{xy}) \quad (4)$$

where, $q = 1.6 \times 10^{-19}$ C is the elementary positive charge; B_z is the transverse magnetic field; and V_{xy}, I_x, and R_{xx} are as defined after Figure 1.

In the case of van der Pauw testing structures employed in this standard (see Figure 2) the results do not depend on the specimen dimensions, which simplifies the measurements and reduces the overall uncertainty of the measurements.

3. Measurement Procedure

3.1. Van der Pauw Sample Geometry

Resistance R_{xx}, R_{xy}, density of charge carriers, n, majority type of charge carriers, and their mobility, μ, can be determined from magneto-resistance measurements of V_{xx}, V_{xy}, I_x, and B_z, using van der Pauw 4 terminal testing structures which are commonly used in development of semiconducting materials and quality control [8, 9].

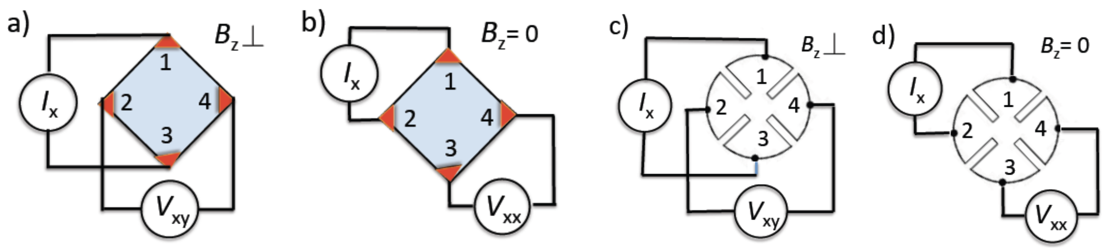

Figure 2. Lay-out of the van der Pauw four terminals testing structures: a) and c) are for measuring Hall resistance, $R_{xy} = V_{xy}/I_x$. Testing structures b) and d) are for measuring Hall sheet resistance, $R_{xx} = V_{xx}/I_x$

The primary advantage of using van der Pauw testing structures (Figure 2) for Hall measurements is their simple four contacts geometry that can be easily implemented for raw materials without need for specialized lithography procedures. In addition, unlike in the case of the Hall bar (Figure1) the specimen dimension and distance between contacts do not need to be known. The typical size of this symmetric square specimen is about 10 mm x 10 mm (the geometrical aspect ratio l/w =1).

Testing samples of nano-scale thin film materials should entail non-magnetic and non-conducting substrates, such as silica or Kapton, with non-magnetic electrical terminals. Dimensions of electrical terminals may be minimized towards point contacts by using, for example, wire bonding. This can reduce variability of contact resistance effects and improve accuracy and reproducibility of the measurement data. The graphene material under test can be deposited by chemical vapor deposition, ink printing, casting from solution etc. In the case of epitaxial graphene or thermally stable free-standing specimens <1 mm thick, electrical contact terminals can be deposited directly on the surface of the film.

The following conditions apply:

1. The sample should have a flat shape and uniform thickness, homogeneous, and isotropic.
2. All contacts should be located at the edge of the sample.
3. The area of any individual contact should be at least an order of magnitude smaller than the area of the sample.

3.2. Measurement of Hall voltage, V_{xy}, and Hall resistance, R_{xy}, using the van der Pauw testing structure (Figure 2a or 2c)

The measurement of Hall voltage (V_{xy}) involves two measurements while the magnetic field B_z is applied:

Measurement of voltage $(V_{xy})_1$ while the constant current, I_x, is sourced at terminals 1,3 of the testing structure (Figures 2a or 2c) and measuring the resulting voltage data at terminals 2,4.

Measurement of voltage $(V_{xy})_2$ by connecting the I_x source to terminals 2,4 and measuring the resulting voltage at terminals 1,2. The V_{xy} value is the average:

$$V_{xy} = [(V_{xy})_1 + V_{xy})_2]/2. \quad (5)$$

$$R_{xy} = V_{xy} / I_x \quad (6)$$

3.3. Measurement of the resistance R_{xx} (sheet resistance) using the van der Pauw method (Figure. 2b or 2d)

Van der Pauw demonstrated [8,9] that there are two characteristic resistances, R_A and R_B, associated with the corresponding terminals shown in Figure 2b. They are related to the sheet resistance R_{xx} through the van der Pauw equation (6):

$$\exp(-\pi R_A/R_{xx}) + \exp(-\pi R_B/R_{xx}) = 1 \quad (7)$$

that can be solved numerically for R_{xx} , where the characteristic resistance R_A and R_B are given by equation (11).

The R_{xx} measurement is carried out at zero magnetic field. It involves application of constant current source, I_x, across the edge of the specimen, between terminals (1,2), and measuring the resulting voltage V_{43} across the opposite edge, at terminals (4,3). The resistance $R_{12,43} = V_{43}/I_{12}$ is calculated from Ohm's law. In the second measurements, current I_x is applied to terminals 2,3 and the resulting voltage drop is read at terminals 1,4. The resistance $R_{23,14} = V_{14}/I_{23}$.

Eight measurements of voltage yield the following eight values of resistance, all of which must be positive:

$$\begin{aligned} R_{21,34} &= V_{34}/I_{21}, \quad & R_{12,43} &= V_{43}/I_{12}, \\ R_{32,41} &= V_{41}/I_{32}, \quad & R_{23,14} &= V_{14}/I_{23} \\ R_{43,12} &= V_{12}/I_{43}, \quad & R_{34,21} &= V_{21}/I_{34}, \\ R_{14,23} &= V_{23}/I_{14}, \quad & R_{41,32} &= V_{32}/I_{41}. \end{aligned} \quad (8)$$

Because the second half of this sequence of measurements is redundant, it permits important consistency checks on measurement repeatability, ohmic contact quality, and sample uniformity.

Measurement consistency following the current reversal requires that:

$$R_{21,34} = R_{12,43}, \qquad R_{32,41} = R_{23,14}$$
$$R_{43,12} = R_{34,21} \qquad R_{14,23} = R_{41,32} \tag{9}$$

The reciprocity theorem requires that:

$$R_{21,34} + R_{12,43} = R_{43,12} + R_{34,21} \quad \text{and}$$
$$R_{32,41} + R_{23,14} = R_{14,23} + R_{41,32} \tag{10}$$

If the left and right sides of (10) fails to be true within 5 % (preferably 3 %), investigate the experimental set-up.

3.4. Calculation of R_{xx} from the two characteristic resistances R_A and R_B:

$$R_A = (R_{21,34} + R_{12,43} + R_{43,12} + R_{34,21})/4 \text{ and}$$
$$R_B = (R_{32,41} + R_{23,14} + R_{14,23} + R_{41,32})/4 \tag{11}$$

Such averaging procedure is based on reciprocity theorem [9] and the benefit is that any offset voltages, such as thermoelectric potentials or potentials due to trapped charges will be cancelled out.

If $R_A = R_B = R_s$ agree to within 5 % or less, then:

$$R_{xx} \approx \pi\, R_s/\ln(2) \tag{12}$$

Otherwise, R_{xx} can be obtained by solving equation (7) numerically for R_{xx} [9, 10].

The measurements of R_A and R_B can be easily automated using a commercial four-point-square DC testing head and a 4-terminal switching board (see Annex A).

Calculate density of charge carriers from the single measurement of I_x and V_{xy} at given B_z preferable on specimen with known n_s

$$n_s = I_x\, B_z/(q\, V_{xy}) \quad [\text{cm}^{-2}] \tag{13}$$

4. Plotting the data, determining Hall coefficient, density and majority of charge carriers

4.1. Hall coefficient, R_H, and density of charge carriers, n_s

Substantial improvement in accuracy and interpretation of the measurements results can be obtained by plotting the Hall Voltage (V_{xy}) as a function of the magnetic field B_z . From the slope of the Hall voltage vs magnetic field, $d(V_{xy})/d(B_z)$:

$$R_H = (1/I_x)\, d(V_{xy})/d(B_z)\ [\text{cm}^2/\text{C}] \qquad (14)$$

$$n_s = I_x / [q\, (d(V_{xy})/d(B_z)]\ [\text{cm}^{-2}] \qquad (15)$$

4.2. Sheet resistance

Use equations 7 or 12 to calculate the R_{xx}.

4.3. Mobility of charge carriers

$$\mu = R_H / R_{xx}\ [\text{cm}^2/\text{Vs}] \qquad (16)$$

The common unit of charge carriers mobility is cm^2/Vs. Even though the system is 2D (e.g., a thin film or electron gas), mobility relates velocity to electric field, not volume. Therefore, dimensionality does not change the unit.

4.4. Majority of charge carriers.

The majority of charge carriers can be determined from the slope of V_{xy} vs B_z plot ($d(V_{xy})/d(B_z)$. In engineering notation, the direction of electric current flow is assigned to the movement of positive charges (*q*). In this notation, the positive slope or positive V_{xy} would indicate that the majority of charge carriers are holes while the negative slope or negative V_{xy} would indicate that the majority of charge carriers are electrons. However, in the scientific notation of Hall effect and Quantum Hall Resistance effect, the elementary charge is the negative charge of an electron (-e), and the sign of equations (1-4) changes and the positive slope of equation (4) indicates that the majority of charge carriers are electrons. (see Annex B)

5. Uncertainty analysis

Plotting the data as a function of B_z, (equations 12-14), followed by linear fitting is the simplest way to eliminate wrong data points and to estimate uncertainty of Hall coefficient, R_H, charge carriers density, n_s, and their mobility, μ. (see example in chapter 8, Figure 4).

For individual measurements of Rxy, Rxx or Vxy that involve multiplication, division, addition or subtraction, the mathematical rules of error propagation are recommended.

When adding or subtracting measurements of quantity z_i, each with uncertainty σ_i , we add the absolute uncertainties in quadrature (the square root of the sum of squares) for standard deviations.

In the case z = x ± y, where x has uncertainty σ_x and y has uncertainty σ_y:

$$\sigma_z = \sqrt{(\sigma_x^2 + \sigma_y^2)}$$

For z = xy or z = x/y such as $R_{xy} = V_{xy}/I_x$, the relative uncertainty of the result equals the quadrature sum of the relative uncertainties of the individual data:

$$(\sigma_z/z)^2 = (\sigma_x/x)^2 + (\sigma_y/y)^2$$

Relative uncertainty (in %) of individual voltage and current measurement may be assumed from the class of particular instrumentation, per manufacturer specification.

The general error propagation formula for a function (f(x, y, z, ...) of independent, random variables uses partial derivatives to determine total uncertainty. For additional guidance see for example Ref. [11].

6. Measurement Report

The report shall include the following:

1. Specimen preparation procedure, geometrical lay-out and the electrical contacts.
2. Figure showing the specimen geometry, dimensions and lay-out of electrical terminals with labeled diagram of electrical quantity being measured [9]
3. Specimen thickness (t) if it can be measured with reasonable uncertainty or estimated.
4. Table of I_x and V_{xy} values measured as a function of $\pm B_z$.
5. Hall Voltage V_{xy}.
6. Sheet resistance, R_{xx}.
7. Charge carriers mobility**,** Hall coefficient R_H
8. The majority of charge carriers
9. Plot of R_{xy} = vs B_z for verification of the possible Hall quantized transport.
10. Uncertainty analysis.

7. Recommended Instrumentation

A typical Hall effect measurement configuration includes the following components:

A constant-current source of a magnitude that's dependent on the sample's resistance. For low resistivity material samples, the source must be able to output current from 1 μA to 0.1 A.

For high resistivity materials (such as intrinsic semiconductors), the constant current source may have to be capable of measurement in the 1nA range

- A high input resistance voltmeter. Depending on the level of material resistivity under test, the voltmeter should enable accurate voltage measurements from 1 μV to 100 V. High resistivity materials may require ultra-high input resistance or differential measurements with lock-in-amplifiers or electrometers with electromagnetic (EM) shielding
- A permanent magnet or an electromagnet. These are typically available with ranges from 0.1 T to 2 T.
  Capability of reversing or scanning reversing the magnetic field within $\pm B_z$ can reduce the uncertainty
- A nonmagnetic sample holder
- A switch matrix and 4-terminals-square sheet resistance probe is recommended to eliminate the need for manual connections/disconnections between probe contacts; it may enable testing multiple samples in the same temp-relative humidity environment. A switch matrix is required if the sample is being tested at cryogenic temperatures
- Hall mobility is dependent on sample temperature and should be monitored during the test

8. Equipment and Configuration for the Hall Effect Measurement using the van der Pauw method

8.1. Example of Instrumentation Configuration for Low-to-High Resistance Range

Figure 3 illustrates the example of instrumentation configuration appropriate for the widest range of sample resistances, from 1 micro-ohm to 1 terra-ohm [11]. A configuration of this type would be most appropriate for characterizing graphene**,** the effects of doping concentration on an intrinsic semiconductor, the effects of doping polymers with increasing amounts of carbon nanotubes. and for studying thin-film photovoltaic materials.

This system configuration shown in Figure 3 employs Keithley's special matrix switching card optimized for Hall effect measurements, the Model 7065, housed in a Model 7001 Switch Mainframe. This card buffers test signals from the sample to the measurement instrumentation and switches current from the current source to the sample taking measurements voltage described by equation 9 in section 5.2 and 5.3. The Model 7065 switching card offers the advantage of unity gain buffers that can be switched in and out to allow the measurement of high resistances by buffering the sample resistance from the meter.

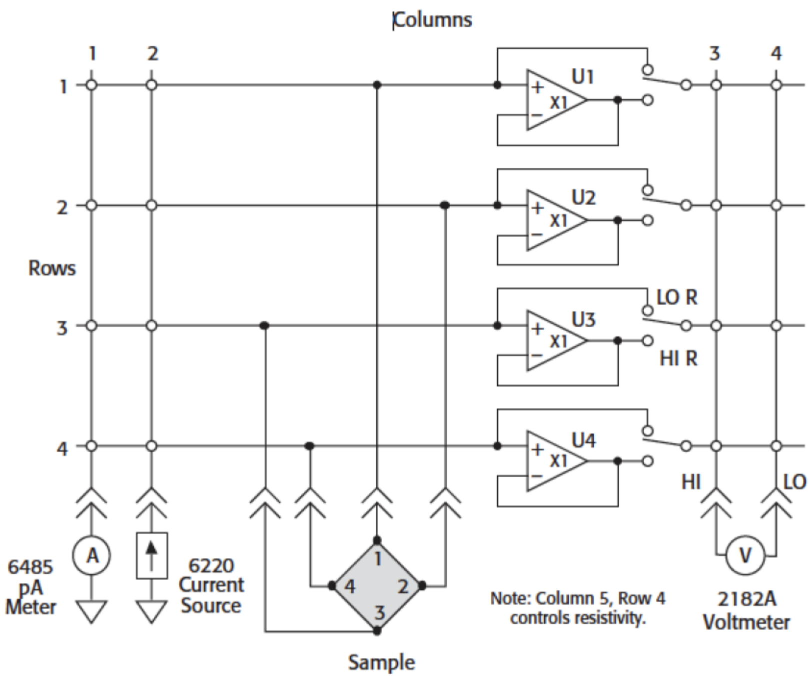

Figure 3**. Example test configuration for characterizing materials with wide range of sample resistances (1 micro-ohm to 1 tera-ohm).**[1]

[1] Certain equipment, instruments, software, or materials are identified in this paper in order to specify the experimental procedure adequately. Such identification is not intended to imply recommendation or endorsement of any product or service by The National Institute of Standards and Technology (NIST), nor is it intended to imply that the materials or equipment identified are necessarily the best available for the purpose.

The Keithley model 6220 and the Keithley model 2182A are designed to work together seamlessly, using a delta mode technique to synchronize their operation and optimize their performance. The delta mode automatically triggers the current source to alternate the signal polarity over the sample terminals and triggers a nanovoltmeter reading at each polarity, cancelling out both constant and drifting thermoelectric offsets, and ensuring the results reflect the true value of the voltage. Once Model 6220 and the Model 2182A are connected properly, all it takes to start a test is pressing the current source's Delta button and then the Trigger button. Model 2182A also provides a second channel of voltage measurement capability, which is useful for monitoring the temperature of the sample. The test setup also includes the Model 6485 Pico-ammeter, the Model 6220 DC Current Source, and the Model 2182A Nanovoltmeter. The Model 6485 Pico-ammeter is included to measure leakage currents, which can either be subtracted out or monitored to evaluate quality of the high resistance measurement. The Model 6220 serves as the constant current source in the configuration shown. By substituting it with the Model 6221 AC+DC Current Source with a built-in arbitrary waveform generator, allows users to make AC Hall effect measurements.

8.2. Enhancing Hall Effect Measurement Confidence

Incorporating multiple good measurement practices into the design of a Hall effect system will increase the likelihood of getting high integrity measurements especially on high resistivity materials [6]:

Always incorporate electrostatic shielding into the system's design to minimize electrical interference, electrostatic coupling, or interference that occurs when an external electric field impinges upon the circuit under test. At low impedance levels, the effects of the interferences usually are not noticeable because any charge that is developed dissipates rapidly. However, high resistance materials do not allow the charge to decay quickly, which may result in unstable measurements. Either DC or AC electrostatic fields may be responsible for these erroneous readings, so always use electrostatic shielding to minimize their effects. As much as practicable, shield the sample being tested and all sensitive measurement circuitry, connect the shield to the low terminal of the test system, and always use shielded cabling. The easiest type of shield to make is a simple metal box or meshed screen that encloses the test circuit. Shielded boxes (a.k.a., Faraday cage) are also available commercially.

Ensure the test system is properly grounded—When there are two or more connections to earth, such as when source and measuring instruments are both connected to a common ground bus, a group loop is formed, which can introduce noise and error voltages. . Frequently, there is a small difference in potential between the ground points, which can cause large currents to circulate and create unexpected voltage drops. A voltage Vg) between the source and instrument grounds will cause a current (Ig) to flow around the loop. This current will create an unwanted voltage in series with the source voltage. Ground loops can occur when more than one instrument is plugged into power strips on different instrument racks. Prevent ground loops from forming by grounding all equipment in the test system at a single point by using isolated power sources and instruments, then establishing a single, good earth-ground point for the entire system. Avoid connecting sensitive instruments to the same ground system used by other instruments, machinery, or other high-power equipment.

Use guarding to reduce the effects of leakage current in the system**.** This includes the use of a guarded current source, guarded voltmeters, and triaxial rather than coaxial cables.

Allow sufficient settling time before making measurements. If you are measuring a high resistance sample, the capacitance in the cabling combined with the high resistance sample creates a large RC time constant, which will cause substantial time delays for voltage levels to reach stable values. To determine the amount of delay time before a voltage level stabilizes, monitor the voltage as a function of time. For example, the voltage on a sample with 1012 Ω resistance may not settle for 20 seconds.

Regularly verify the system's performance. The simplest way to do this is to build a test structure using four resistors of equal value that are similar in magnitude to the resistance of the sample under test and use this as a basis for comparison. It is recommended to compare your results with those from a calibrated "golden sample" , such as a NIST characterized sample, to validate your measurement results.

Minimize sources of thermoelectric voltages. Whenever possible, use the same materials in all connections, such as all copper connections and copper wire. Reverse the current source's polarity and average the readings to eliminate EMF errors. Always allow the test equipment to warm up and reach thermal equilibrium before the start of testing and minimize temperature gradients across the sample.

9. Laboratory case study: Hall resistance measurement examples of graphene ink and epitaxial graphene – with quantum Hall effect

9.1. Materials

Graphene ink was prepared from commercially available graphene nanoplates dispersed in solution of ethyl cellulose in ethanol and shear mixed in a high shear mixer. The resulting dispersion was centrifuged and purified as described in [7]. Films, 500 nm thick were obtained by ink printing onto un-doped silicon wafers having 300 nm SiO_2 insulating layer on top. Specimens were diced to 8 mm x 8 mm for Hall measurements. Electrical terminals were made by sputtering gold through a shadow mask onto and extended by gold wire bonding.

Single-layer epitaxial graphene on the Si-terminated face (SiC/G) was grown on high purity 4H-SiC(0001) 330 μm thick wafers. The wafers were diced to obtain specimen size of 7.8 mm $\times$ 7.8 mm. The substrates were then annealed at 1900°C in Argon at (101-105) kPa using a controlled Si sublimation process, which stops at one single-layer on Si-terminated face [14]. Electrical terminals were made by sputtering Gold through a precision shadow mask onto on the graphene surface and extended by gold wire bonding.

9.2. Hall measurements

For compatibility with quantum resistance measurement, the data in Figure 4 are plotted in scientific notation where the elementary charge is negative electron (–e). Hall voltage and Hall resistance were measured using conventional van der Pauw square geometry (Figure 2a and b) having length to width aspect ratio of 1. The Hall voltage data (V_{xy}) vs magnetic flux density B_z for graphene ink is shown in Figure 4.

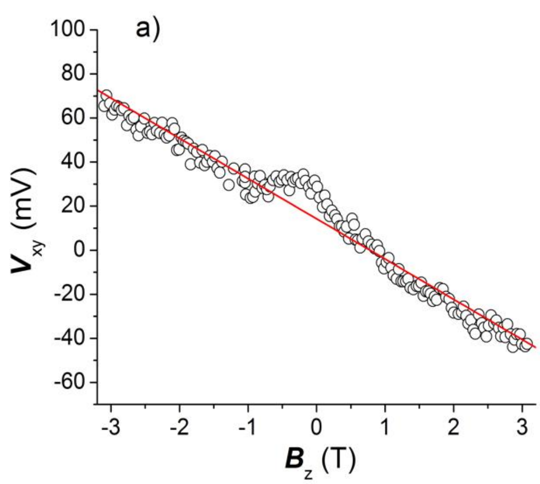

Figure 4. Graphene ink; (a) Hall voltage V_{xy} measured as a function of magnetic field (B_z) The solid line represents the linear fit thru the data points (symbols). The negative slope indicates that the majority of charge carriers are positive holes.

The slope of the fitted straight line in Figure 4 is –0.0183 ± 3 x10^{-4} V/T. The negative slope indicates that the majority of charge carriers are positive holes. The corresponding number of charge carriers from equation (13), n ≈ 3.4 x 10^{14} cm^{-2}. Similarly, using the applied current, I_x =1 x10^{-6} A, and the resistance R_{xx} (B_z=0) ≅ 136.5 Ω, the mobility of charge carriers from equation (16) μ = 135 cm^2/Vs. Trapped charge carriers within the conducting band are seen at B_z≈ 0. There is no evidence that the Hall resistance R_{xy} in graphene inks is quantized, when compared to R_{xy} plot in Figure 5 for epitaxial single graphene.

Figure 6 shows Hall resistance, R_{xy}, measured for epitaxial graphene as a function of magnetic field B_z. The R_{xy} plot evidences the exact quantum Hall resistance, at the Landau filing factors ν ±2, where the extended R_{xy} plateau acquire the quantized value of $h/2e^2 \approx 12.906$ kΩ.

The positive slope of R_{xy}) in the B_z vicinity of ± 2T, indicates that the majority of charge carriers are electrons, and that the conductivity of single layer epitaxial graphene is metallic. From equation (13) the concentration of charge carriers (n) is in the range of 2.98×10^{11} cm^{-2}. From equation (14) the mobility of electrons is in the range 7.91×10^3 $cm^2V^{-1}s^{-1}$.

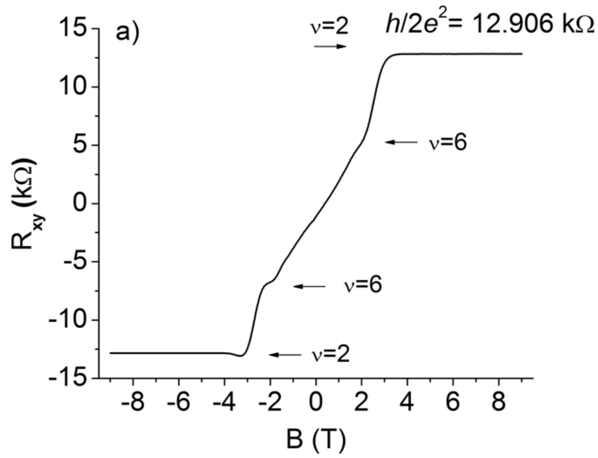

Figure 5. Epitaxial; graphene; Hall resistance (R_{xy} = V_{xy} /I_x) for epitaxial graphene as a function of magnetic field (B_z).The charge transport is quantized showing quantum resistance plateau R_{xy} = h/2e^2=12.906 kΩ.
The positive slope of R_{xy} indicates that the majority of charge carriers are electrons.

The observed signatures of the quantized charge transport provide evidence that the epitaxial graphene is truly a 2D materials with single-layer signature [14].

9.3. Uncertainty analysis

The combined standard uncertainty of the presented charge transport parameters was obtained from the general formula for the error propagation model using standard errors from the least-squares linear fitting through data points or by using maximum errors of the measured values [15].

In the case of the charge carriers mobility in Figure 4 the uncertainty from the linear fit of the slope $d(R_{xy})/d(B_z)$ = 3 x10^{-4} V/T. The ΔR_{xx} = ± 0.2 Ω and the error ΔI_x = ± 5 x10^{-8} A. The combined relative uncertainty of grapheme ink mobility $\Delta\mu/\mu$ = 5.4 %, $\Delta n/n$ = 5%. In comparison, the combined relative uncertainty of the quantized resistance shown in Figure 5 is below 0.01 %.

10. References

[1] Jeffrey Lindemuth, Hall Effect Measurement Handbook. A fundamental Tool for Semiconductor Chracterization. Brad C. Dodril Editor, https://www.lakeshorecryotronics.com/hall-effect-measurement-handbook-pdf

[2] Hall Measurement using the van der Pauw method, NIST standard, https://www.nist.gov/pml/nanoscale-device-characterization-division/popular-links/hall-effect/resistivity-and-hall

[3] ASTM F76-08 Standard Test Methods for Measuring Resistivity and Hall Coefficient and Determining Hall Mobility in Single-Crystal Semiconductors. https://store.astm.org/f0076-08.html.

[4] Simple analytical method for determining electrical resistivity and sheet resistance using the van der Pauw procedure. F. S. Oliveira, R. B. Cipriano, F. T. da Silva, E. C. Romão & C. A. M. dos Santos, *Scientific Reports* **volume 10**, Article number: 16379 (2020)

[5] M. Kruskopf, R. E. Elmquist, *Epitaxial graphene for quantum resistance metrology*, Metrologia vol. 55, R27 (2018.

[6] Robert Green, Senior Market Development Manager Keithley Instruments, Inc, *Hall Effect Measurements in Materials Characterization,* https://download.tek.com/document/HallEffect_WhtPapr.pdf?_gl=1*dvvm5x*_ga*MTA5NzgyODU1LjE3NjMzMTE3MjE.*_ga_1HMYS1JH9M*czE3NjMzMTE3MjEkbzEkZzEkdDE3NjMzMTE4NjQkajYwJGwwJGgw.

[7] C. M. de Moraes, Jan Obrzut et al, Elucidating charge transport mechanism in cellulose stabilized graphene inks, J. Materials Chem. C, vol. 8, p. 15086 (2020

[8] Conor O'Brien, Graphene Market & 2D Materials Assessment 2024-2034: Technologies, Markets, Players, IDTechEX https://www.idtechex.com/en/research-report/graphene-market-and-2d-materials-assessment-2024-2034-technologies-markets-players/967.

[9] J. Obrzut, Graphene: A new Horizon for Modern Technology, *NEMA Electroindustry*, September 2011, page 9.

[10] The Graphene Council, The 2020 Graphene Survey, 04 Jan 2021 https://cdn.ymaws.com/www.thegraphenecouncil.org/resource/resmgr/2020_survey/2020_Survey_Report.pdf

[11] Kirkup, L.; Frenkel, B. *An Introduction to Uncertainty in Measurement*; Cambridge University Press, Cambridge, UK, 2006.